QUANTIFYING THE INFLUENCE OF INTENSITY CHANNELS FROM POLSAR IMAGES FOR EDGE DETECTION ON INFORMATION FUSION

Anderson A. de Borba[a], Maurício Marengoni[b], and Alejandro C. Frery[c].

[a]IBMEC-SP, Alameda Santos, 2356 - Jardim Paulista, SP – Brazil,
[b]Departamento de Ciência da Computação, Universidade Federal de Minas Gerais, MG – Brazil,
[c]School of Mathematics and Statistics, Victoria University of Wellington, 6140, New Zealand.

ABSTRACT

A prompt and effective response to natural disasters is essential. Polarimetric Synthetic Aperture Radar (PolSAR) images play a crucial role in helping decisions in these scenarios, especially in adverse weather or the absence of sunlight. In this context, PolSAR images still provide information. In these situations, the process of finding precise boundaries to determine the extent of the disaster is an essential issue as PolSAR image resolutions are usually high (of the order of $10\,\mathrm{m}$). The fusion of information from the intensity channels of PolSAR images for edge detection enhances the precision of edges presented in these images. In this work, we propose three metrics: the accuracy (Mac), the F_1-score (Mfe), and the Matthews correlation coefficient normalized (nMcc). These metrics quantify the influence of the information from the intensity channels of PolSAR images on the information fusion process for edge detection.

***Index Terms*—** Metrics, information fusion, edges detection, PolSAR, maximum likelihood estimation.

1. INTRODUCTION

Natural disasters such as earthquakes or flooding have great destructive power. Among the consequences are the economic impact in the affected area and the loss of human lives. In the latter case, prompt and effective responses are required to reduce the number of losses and the precision of determining the affected area. However, current knowledge and technology can not predict natural disasters with enough time to take proper measures, which becomes a problem.

Among the consequences of natural disasters are the collapse of debris and rapid flooding, which can cause material losses and threaten human lives. In this context, the remote sensing area has increased its importance in analyzing the affected area and get information to assist in rescue missions.

However, if the disaster happens at night or under severe weather conditions, optical images cannot provide adequate information. In these cases, we can use PolSAR images, which can acquire information under these conditions.

In this context, the automatic and precise detection of risk areas or the flood's evolution becomes important. Further information can be found in Refs. [1–3].

To assist in the risk alarm process and delimit precisely the affected area and help people's rescue in regions with natural disasters, edge detection in PolSAR images is essential. The work presented here quantifies each intensity channel's influence in the process of edge detection based on the fusion of information as presented in Ref. [4].

The article is structured as follows. Section 2 describes the statistical modeling for PolSAR date. Section 3 describes the Gambini Algorithm (GA) to edge detection in each intensities channels. Section 4 describes the approaches for fusing edge evidences. Section 5 describes the metrics. Section 6 presents the results. In Section 7 we discuss the results.

2. STATISTICAL MODELING FOR POLSAR DATA

Multi-looked fully polarimetric data follows the Wishart distribution with PDF defined by:

$$f_{\mathbf{Z}}(\mathbf{z};\boldsymbol{\Sigma},L)=\frac{L^{pL}|\mathbf{z}|^{L-p}}{|\boldsymbol{\Sigma}|^{L}\Gamma_p(L)}\exp\big\{-L\,\mathrm{tr}(\boldsymbol{\Sigma}^{-1}\mathbf{z})\big\},\qquad(1)$$

where $\mathbf{z}$ is a positive-definite Hermitian matrix, L is the number of looks, $\mathrm{tr}(\cdot)$ is the trace operator of a matrix and $\Gamma_p(L)$ is the multivariate Gamma function defined by $\Gamma_p(L)=\pi^{\frac{1}{2}p(p-1)}\prod_{i=0}^{p-1}\Gamma(L-i)$, where $\Gamma(\cdot)$ is the Gamma function. In this study we used three channels ($p=3$). This situation is denoted by $\mathbf{Z}\sim W(\boldsymbol{\Sigma},L)$, which satisfies $E[\mathbf{Z}]=\boldsymbol{\Sigma}$.

Since we are interested on describing the information conveyed by parts of this matrix under the Wishart model, we use the fact that each intensity channel follows a Gamma law with probability density function

$$f_Z(z;\mu,L)=\frac{L^L z^{L-1}}{\mu^L\Gamma(L)}\exp\big\{-Lz/\mu\big\},\quad z>0,\qquad(2)$$

e-mail:[a]anderson.aborba@professores.ibmec.edu.br,
[b]mmarengoni@hotmail.com, [c]alejandro.frery@vuw.ac.nz

where $L > 0$, and $\mu > 0$ is the mean. The log-likelihood of the sample $\boldsymbol{z} = (z_1, \ldots, z_n)$ under this model is

$$\mathcal{L}(\mu, L; \boldsymbol{z}) = n\big[L\ln(L/\mu) - \ln\Gamma(L)\big] + L\sum_{k=1}^{n}\ln z_k - \frac{L}{\mu}\sum_{k=1}^{n} z_k. \tag{3}$$

We obtain $\big(\widehat{\mu}, \widehat{L}\big)$, the maximum likelihood estimator (MLE) of (μ, L) based on $\boldsymbol{z}$, by maximizing (3) with the BFGS (Broyden-Fletcher-Goldfarb-Shanno) method [5].

3. EDGE DETECTION ON A SINGLE DATA STRIP

The GA estimates the point at where sample properties change. It has been used with stochastic distances [6], and with the likelihood function [7, 8] for edge detection in SAR/PolSAR images. It can be adapted to any suitable measure of dissimilarity between two samples.

The algorithm starts by casting rays from a point inside the candidate region, e.g., the centroid. Data are collected around each ray to form the sample $\boldsymbol{z} = (z_1, z_2, \ldots, z_n)$, which is partitioned at position j:

$$\boldsymbol{z} = (\underbrace{z_1, z_2, \ldots, z_j}_{\boldsymbol{z}_\mathrm{I}}, \underbrace{z_{j+1}, z_{j+2}, \ldots, z_n}_{\boldsymbol{z}_\mathrm{E}}).$$

We assume two (possibly) different models for each partition: $\boldsymbol{Z}_\mathrm{I} \sim \Gamma(\mu_\mathrm{I}, L_\mathrm{I})$, and $\boldsymbol{Z}_\mathrm{E} \sim \Gamma(\mu_\mathrm{E}, L_\mathrm{E})$. We then estimate $(\mu_\mathrm{I}, L_\mathrm{I})$ and $(\mu_\mathrm{E}, L_\mathrm{E})$ with $\boldsymbol{z}_\mathrm{I}$ and $\boldsymbol{z}_\mathrm{E}$, respectively, by maximizing (3), and obtain $\big(\widehat{\mu}_\mathrm{I}, \widehat{L}_\mathrm{I}\big)$ and $\big(\widehat{\mu}_\mathrm{E}, \widehat{L}_\mathrm{E}\big)$.

Afterward, we compute the total log-likelihood of $\boldsymbol{z}_\mathrm{I}$ and $\boldsymbol{z}_\mathrm{E}$:

$$\begin{aligned}\mathcal{L}\big(j; \widehat{\mu}_I, \widehat{L}_I, \widehat{\mu}_E, \widehat{L}_E\big) = &-\left(\frac{\widehat{L}_\mathrm{I}}{\widehat{\mu}_\mathrm{I}}\sum_{k=1}^{j} z_k + \frac{\widehat{L}_\mathrm{E}}{\widehat{\mu}_\mathrm{E}}\sum_{k=j+1}^{n} z_k\right) + \\ &j\big[\widehat{L}_\mathrm{I}\ln(\widehat{L}_\mathrm{I}/\widehat{\mu}_\mathrm{I}) - \ln\Gamma(\widehat{L}_\mathrm{I})\big] + \widehat{L}_\mathrm{I}\sum_{k=1}^{j}\ln z_k + \\ &(n-j)\big[\widehat{L}_\mathrm{E}\ln(\widehat{L}_\mathrm{E}/\widehat{\mu}_\mathrm{E}) - \ln\Gamma(\widehat{L}_\mathrm{E})\big] + \widehat{L}_\mathrm{E}\sum_{k=j+1}^{n}\ln z_k,\end{aligned} \tag{4}$$

and estimate the edge position on the ray which is the coordinate $\widehat{j}$ that maximizes it, for this, Generalized Simulated Annealing (GenSA [9]) was used. De Borba et al [4] present the edge detection pseudo-code Gambini Algorithm.

4. FUSION OF EVIDENCES

Assume we have n_c binary images $\{\widehat{\boldsymbol{j}}_c\}_{1\le c\le n_c}$ in which 1 denotes an estimate of edge and 0 otherwise. They all have size $m \times n$. These images will be fused to obtain the binary image I_F. Fig 1 shows the scheme for evidence fusion.

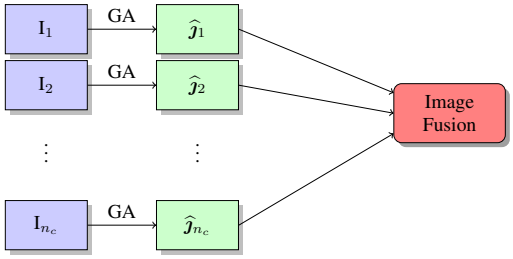

Fig. 1. Fusion Scheme

We compare the results of six fusion techniques: simple average, multi-resolution discrete wavelet transform (MR-DWT), principal components analysis (PCA), ROC statistics, multi-resolution stationary wavelet transform (MR-SWT), and multi-resolution singular value decomposition (MR-SVD). Fig. 2 illustrates the process of information fusion. For more details see Ref. [4].

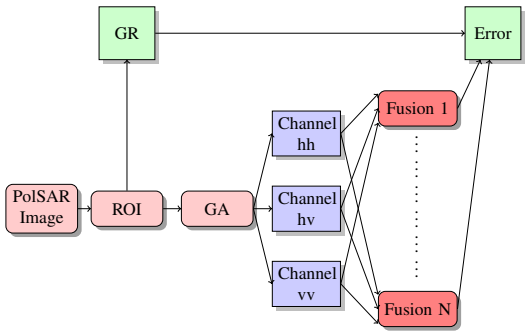

Fig. 2. Flowchart of the evidence fusion process

5. METRICS

This section is based on Refs. [10, 11]. The quality metrics are built on the confusion matrix of the binary images, compared with the Ground Reference image (GR). We consider the positive instance by p (pixel value 1), and the negative instance by n (pixel value 0). The instances are classified as: TP: a pixel detected as an edge is on the edge in the GR image, FN: a pixel on the edge in the GR image is not detected, TN: a pixel detected not on the edge is not on the edge in the GR image, and FP: a pixel not on the edge in GR image is detected as an edge.

We used the following metrics:

$$\mathrm{Mac} = \frac{\mathrm{TP}+\mathrm{TN}}{\mathrm{TP}+\mathrm{TN}+\mathrm{FP}+\mathrm{FN}},$$

$$F1\text{-score} = \frac{2\mathrm{TP}}{2\mathrm{TP}+\mathrm{FP}+\mathrm{FN}},$$

$$\mathrm{nMcc} = \frac{\frac{\mathrm{TP}\cdot\mathrm{TN}-\mathrm{FP}\cdot\mathrm{FN}}{\sqrt{(\mathrm{TP}+\mathrm{FP})\cdot(\mathrm{TP}+\mathrm{FN})\cdot(\mathrm{TN}+\mathrm{FP})\cdot(\mathrm{TN}+\mathrm{FN})}}+1}{2}.$$

All metrics are scaled between 0 (worst case) and 1 (best case).

6. RESULTS

The system presented here was executed on a Intel© Core i7-9750HQ CPU 2.6 GHz 16 GB RAM computer.

Fig. 3(a) shows a 750×1024 pixels AIRSAR (Airborne Synthetic Aperture Radar) PolSAR image of Flevoland, L-band, with the radial lines where edges are detected. Fig. 3(b) shows the ground reference in red.

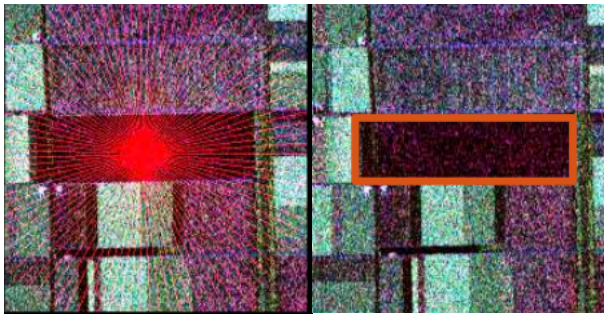

(a) Image and rays. (b) Ground reference

Fig. 3. ROI to Flevoland image in Pauli decomposition, and ground reference

Figs. 4(a), 4(b), and 4(c) show, respectively, the edge evidences in the hh, hv and vv channels as obtained by MLE.

It is worth noting that GenSA has accurately identified the maximum value of $\mathcal{L}$ (Eq. (4)), even in the presence of multiple local maxima. A visual assessment leads to conclude that the best results are provided by hv, although with a few outlier points.

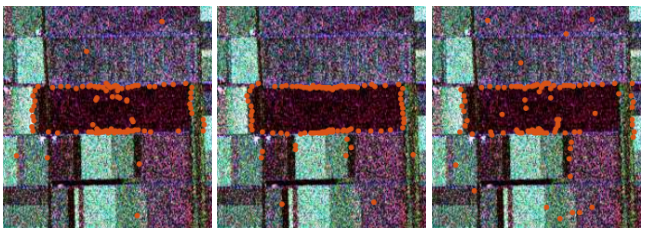

(a) Channel hh (b) Channel hv (c) Channel vv

Fig. 4. Images show edges evidences from the three intensity channels using the MLE method

Figs. 5a, 5b, 5c, 5d, 5e, and 5f show the results of fusing these evidences.

Simple average and PCA produce similar results. MR-SVD produces considerably fewer outliers than the other methods. ROC produces accurate edges, with few outliers,

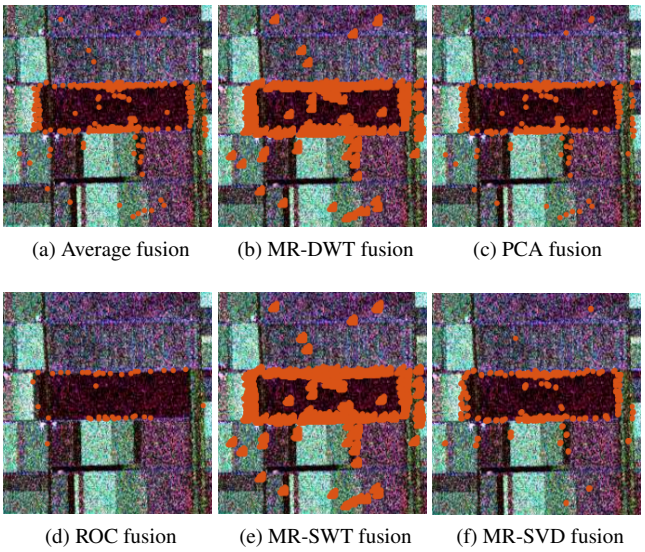

(a) Average fusion (b) MR-DWT fusion (c) PCA fusion

(d) ROC fusion (e) MR-SWT fusion (f) MR-SVD fusion

Fig. 5. Images show the results of applying the six fusion methods after finds edges evidences in intensities channels

but sparsely. Both wavelet-based methods (DWT and SWT) produce too dense edges and many outliers.

The method for detecting edge evidence was implemented in R. The fusion and other methods were implemented in Matlab. Following the guidelines presented in Ref. [12], code and data are available at `https://github.com/anderborba/igarss_2021_bmf`.

We computed the error comparing the methods' results and their fusion with the GR image. We found the confusion matrix to compute accuracy, F_1-score, and Matthews correlation coefficient metrics. Figures 6a, 6b and 6c show the relative performance of the metrics taking as reference the worst result found.

7. DISCUSSION

According to Mac, the methods showed excellent performance because the datasets (images) with methods results are unbalanced; that is, the number of TNs is much larger than the number of TPs, FPs, and FNs. The worst measure was MR–SWT (99.33 %), and the best was ROC (91.04 % higher). The metric correctly measures the edges evidence in the intensities channels. However, it is inconclusive to order the channels in a degree of importance in the fusion of information. A visual inspection of Fig. 5(d) reveals that the fusion using ROC is sparse because the technique detects few FP and FN.

The methods have low performance, according to Mfe, primarily because Mfe does not consider the TN points, and the number of points found in each radial line can be higher than 1. The worst case is ROC, whose value is 1.39 %, and the best approach is MR–DWT with a performance 11.65 %

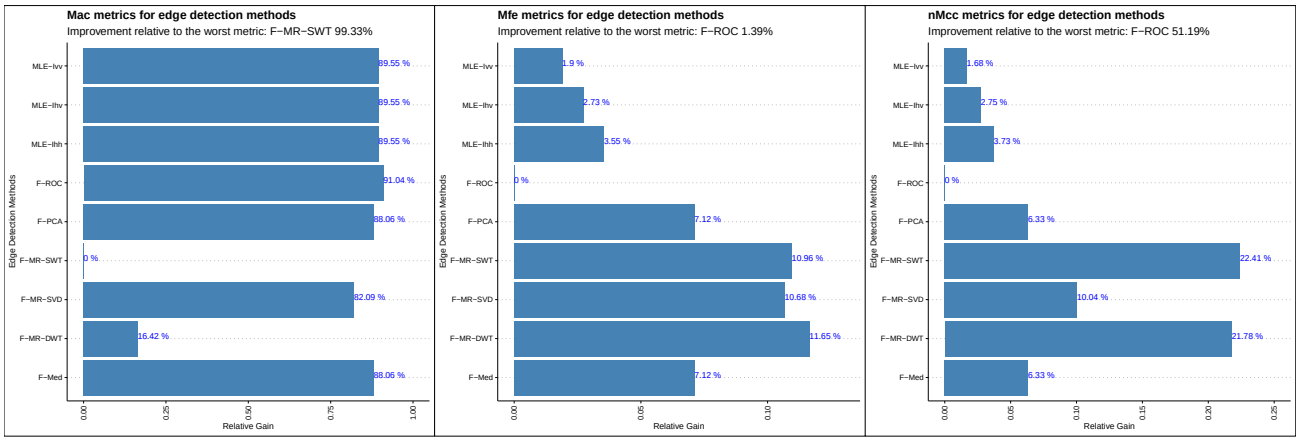

(a) Mac (b) Mfe (c) nMcc

Fig. 6. The figures show the measures of quality applied in the MLE methods and the Fusion methods

higher. Mfe can be used to order the intensity channels. For example, we can say that I_{hh} has the best performance with the MLE. Mfe assigns low performance to high values of FP and FN compared to TP.

The worst method under the nMcc metric is also ROC: $51.19\,\%$, and the best result was recorded for MR–SWT ($22.41\,\%$ higher). nMCC can also rank the intensity channels in order of importance.

We conclude that accuracy does not provide information on the intensity channels or in the information fusion process. At the same time, Mfe and nMcc metrics allow for an ordering of the intensity channels and decide the channels to be used in the fusion process. Therefore we can quantify the influence of intensity channels on the process of fusing information for edge detection in PolSAR images.

8. REFERENCES

[1] W. Zhai, C. Huang, and W. Pei, "Building damage assessment based on the fusion of multiple texture features using a single post-earthquake PolSAR image," *Remote Sens.*, vol. 11, no. 8, p. 897, 2019.

[2] W. Zhai, H. Shen, C. Huang, and W. Pei, "Fusion of polarimetric and texture information for urban building extraction from fully polarimetric SAR imagery," *Remote Sensing Letters*, vol. 7, no. 1, pp. 31–40, 2016.

[3] H. Cao, H. Zhang, C. Wang, and B. Zhang, "Operational flood detection using Sentinel-1 SAR data over large areas," *Water*, vol. 11, no. 4, p. 786, 2019.

[4] A. A. De Borba, M. Marengoni, and A. C. Frery, "Fusion of evidences in intensities channels for edge detection in PolSAR images," *IEEE Geosci. Remote Sens. Lett.*, in press.

[5] A. Henningsen and O. Toomet, "maxlik: A package for maximum likelihood estimation in R," *Computational Statistics*, vol. 26, no. 3, pp. 443–458, 2011.

[6] A. Nascimento, M. Horta, A. Frery, and R. Cintra, "Comparing edge detection methods based on stochastic entropies and distances for PolSAR imagery," *IEEE J. Sel. Top. Appl. Earth Obs. Remote Sens.*, vol. 7, no. 2, pp. 648–663, 2014.

[7] J. Gambini, M. Mejail, J. Jacobo-Berlles, and A. C. Frery, "Feature extraction in speckled imagery using dynamic B-spline deformable contours under the G0 model," *Int. J. Remote Sens.*, vol. 27, no. 22, pp. 5037–5059, 2006.

[8] A. C. Frery, J. Jacobo-Berlles, J. Gambini, and M. Mejail, "Polarimetric SAR image segmentation with B-Splines and a new statistical model," *Multidimension. Syst. Signal Process.*, vol. 21, pp. 319–342, 2010.

[9] Y. Xiang, S. Gubian, B. Suomela, and J. Hoeng, "Generalized Simulated Annealing for Global Optimization: The GenSA Package," *The R Journal*, vol. 5, no. 1, pp. 13–28, 2013.

[10] D. Chicco and G. Jurman, "The advantages of the Matthews correlation coefficient (MCC) over F1 score and accuracy in binary classification evaluation," *BMC Genomics*, vol. 21, 2020.

[11] P. Branco, L. Torgo, and R. P. Ribeiro, "A survey of predictive modeling on imbalanced domains," *ACM Comput. Surv.*, vol. 49, no. 2, Aug. 2016.

[12] A. C. Frery, L. Gomez, and A. C. Medeiros, "A badging system for reproducibility and replicability in remote sensing research," *IEEE J. Sel. Top. Appl. Earth Obs. Remote Sens.*, vol. 13, pp. 4988–4995, 2020.